Design of AlGaN/AlN Dot-in-a-Wire Heterostructures for Electron-Pumped UV Emitters

Ioanna Dimkou, Anjali Harikumar, Akhil Ajay, Fabrice Donatini, Edith Bellet-Amalric, Adeline Grenier, Martien den Hertog, Stephen Purcell, Eva Monroy

Design of AlGaN/AlN dot-in-a-wire heterostructures for electron-pumped UV emitters

*Ioanna Dimkou, Anjali Harikumar, Akhil Ajay, Fabrice Donatini, Edith Bellet-Amalric, Martien I. den Hertog, Stephen T. Purcell, and Eva Monroy**

I. Dimkou
Univ. Grenoble-Alpes, CEA-Leti, 17 av. des Martyrs, 38000 Grenoble, France

A. Harikumar, Dr. A. Ajay, Dr. E. Bellet-Amalric, Dr. E. Monroy
Univ. Grenoble-Alpes, CEA-IRIG-DEPHY-PHELIQS, 17 av. des Martyrs, 38000 Grenoble, France
E-mail: eva.monroy@cea.fr

Dr. F. Donatini, Dr. M. I. den Hertog
Univ. Grenoble-Alpes, CNRS-Institut Néel, 25 av. des Martyrs, 38000 Grenoble, France

Dr. S. T. Purcell
Univ. Lyon, Université Claude Bernard Lyon 1, CNRS, Institut Lumière Matière, 69622 Lyon, France

Keywords: ultraviolet, nanowires, AlGaN, quantum dot, lamp

This paper describes the fabrication of nitrogen-polar $Al_xGa_{1-x}N$/AlN (x = 0, 0.1) quantum dot superlattices integrated along GaN nanowires for application in electron-pumped UV sources. The nanowires are grown using plasma-assisted molecular-beam epitaxy on n-type Si(111) wafers using a low-temperature AlN nucleation layer. Growth conditions are tuned to obtain a high density of non-coalesced nanowires. To improve the uniformity of the height along the substrate, the growth begins with a base long nanowire (~900 nm), with a diameter of 30-50 nm. The $Al_xGa_{1-x}N$/AlN active region is 400 nm long (88 periods of quantum dots), long enough to collect the electron-hole pairs generated by an electron beam with an acceleration voltage ≤ 5 kV. The spectral response is tuned in the 340 to 258 nm range by varying the dot/barrier

thickness ratio and the Al content in the dots. Internal quantum efficiencies as high as 63% are demonstrated.

1. Introduction

UV light emitting diodes (LEDs) are in demand for disinfection purposes[1] at specific wavelengths. They also offer lower power consumption, the potential for longer lifetime, lower voltage requirement and non-toxic waste after use, as opposed to their mercury lamp counterparts. AlGaN is the material of choice for this technology because of its direct bandgap and the possibility to dope it both n-type and p-type [2,3]. Having said that, such devices have not reached their industrial maturity yet due to drawbacks in terms of electrical injection and light extraction, which limit their wall-plug efficiency [4].

A promising alternative for the fabrication of highly efficient, eco-friendly UV lamps is based on the injection of electrons into AlGaN/AlN nanostructures using a miniaturized electron gun, e.g. a carbon nanotube cathode. Such a configuration avoids the problems associated with the carrier injection (dopant ionization energy, asymmetric carrier mobility of electrons and holes, realization of ohmic contacts). Furthermore, the electron injection efficiency is wavelength-independent in the UV range, so it should be possible to fabricate lamps operating close to the AlN band gap (e.g. 210 nm) without degradation of the efficiency.

Electron-pumped emission from GaN and AlGaN quantum wells has been reported [5–9], but such lamps displayed low wall plug efficiency mostly due to the poor light extraction efficiency. Furthermore, lasing around 350 nm has been demonstrated in electron-pumped GaN/AlGaN ridge structures under pulsed pumping [10,11]. For the implementation of such electron-pumped UV sources, the semiconductor geometry and conductivity must be adapted to maximize the energy conversion, light extraction and charge evacuation. There are several motivations to consider nanowires (NWs) for this application. First, their as-grown shape spontaneously favors light extraction [12], without additional processing requirements. In addition, the relatively easy implementation of three dimensionally confined objects (dots in a wire) results in high values of internal quantum efficiency (IQE) at room temperature [13]. Last

but not the least, their direct growth self-assembled on silicon substrates reduces the cost of the system.

One of the main challenges for the growth of NW ensembles for electron-pumped UV sources is the homogeneity of the dot thickness and composition along an active region that is hundreds-of-nm long. It is known that the luminescence from GaN/AlGaN and AlGaN/AlN superlattices (SLs) on GaN NWs presents strong spectral dispersion, with broad and sometimes multi-line spectral profiles [14,15]. Such dispersion is due the variation of the dot height and diameter along the growth axis [16–18], the different strain relaxation in the dots along the growth axis [16,17,19], the presence of monolayer thickness fluctuations in the dots [16], and the alloy inhomogeneities and inter-diffusion phenomena at the hetero-interfaces, which depend on the strain state of the structure [15]. Additional perturbations can be introduced by coalesced areas and lateral GaN inclusions [20]. It is hence highly important to develop precisely controlled growth processes that allow the synthesis of homogeneous AlGaN/AlN quantum dot SLs in a NW geometry.

In this work, we describe the growth and characterization of N-polar $Al_xGa_{1-x}N$/AlN (x=0, 0.1) quantum dot SLs grown as extensions on GaN NWs and designed for their application in electron-pumped UV sources. The NWs are grown using plasma-assisted MBE on n-type Si(111) wafers using a low temperature AlN nucleation layer. Growth conditions are tuned to obtain a high density of non-coalesced GaN NWs. On top of them, the $Al_xGa_{1-x}N$/AlN active region is 400 nm long (88 periods of quantum dots). Such structures present single-line spectral emission with IQE that can reach 63%.

2. Results and discussion

Self-assembled N-polar GaN NWs were synthesized using plasma-assisted molecular beam epitaxy (PAMBE) on n-type Si(111) substrates using a low-temperature AlN nucleation layer, as described elsewhere [21,22]. To improve the height uniformity [23], the growth began with a

long (~900 nm) NW base with a diameter of 30-50 nm, grown under N-rich conditions (Ga/N flux ratio: $\Phi_{Ga}/\Phi_N = 0.25$) at a substrate temperature $T_S = 810°C$ and at a growth rate $v_G = 330$ nm/h. This was followed by the deposition of a 400-nm-long $Al_xGa_{1-x}N$/AlN (x = 0, 0.10) SL, i.e. 88 periods of quantum dots. The $Al_xGa_{1-x}N$ dots were grown using the same Ga flux as for the NW base, and adding an Al flux $\Phi_{Al} = x/v_G$, where x is the targeted Al mole fraction. The AlN sections were grown at the stoichiometry ($\Phi_{Al}/\Phi_N = 1$). The whole SL was synthesized without any growth interruption. To adjust the spectral response, we varied the dot/barrier thickness ratio and the Al content in the dots, maintaining the number of periods (88) and the period length (4.5 nm) constant.

Figure 1(a) presents a typical scanning electron microscopy (SEM) image of the cross section of an as-grown sample of GaN NWs containing an $Al_xGa_{1-x}N$/AlN SL, e.g. the image corresponds to a sample with 88 periods of $Al_{0.1}Ga_{0.9}N$ / AlN (0.75 nm / 3.75 nm). The NWs are detached from each other, but highly packed. Top view images point to a NW density of 6-8×10^9 cm^{-3}. The NW diameter is in the range of 30-50 nm at the base, increasing to 50-70 nm in the top region due to the enhancement of lateral growth when depositing AlN [24,25].

The as-grown NW ensemble was characterized using x-ray diffraction (XRD) in order to validate the periodicity of the structure, with the results illustrated in **Figure 1(b)**. These measurements provide average information over a surface of several millimeters squared, and are hence sensitive to the dispersion of tilts and twists in the NW ensemble. Several satellites of the (0002) reflection of the SL are resolved, which confirms the thickness uniformity along the growth axis and the reproducibility of the period length from sample to sample (period = 4.3±0.2 nm). It should be noticed that the (0002) reflection of GaN originated by the NW base is not located at the angular position of relaxed GaN ($2\theta = 34.57°$), but at slightly larger angles.

To get highly resolved information on the NW structure, the NWs were dispersed on holey carbon membranes for scanning transmission electron microscopy (STEM) observations.

Figure 2(a-b) presents high-angle annular dark field (HAADF) STEM images of a GaN/AlN (1.5 nm / 3.0 nm) SL (88 periods) on a GaN NW. The dots display regular thickness along the NW, and the whole GaN/AlN SL is enveloped by an AlN shell. **Figure 2(c)** shows a high magnification HAADF-STEM view of an $Al_{0.1}Ga_{0.9}N$/AlN (0.65 nm / 3.85 nm) SL, which confirms the nominal layer thicknesses and the homogeneity of the structure. In both samples, we observe a decrease of the thickness of the AlN shell along the growth axis, which is more important in the sample with higher Al content in the SL. This is consistent with the fact that the AlN shell forms as a result of the low mobility and of the Al atoms impinging on the NW sidewalls. From STEM analysis of various NWs, the thickness of the shell is estimated to be only 1-2% of the axial AlN thickness. The presence of the AlN shell imposes a uniaxial compressive stress to the GaN base, which justifies the shift of the GaN (0002) XRD reflection as observed in **Figure 1(b)**.

Optical characterization by cathodoluminescence (CL) at room temperature, with an electron acceleration voltage V_A = 5 kV, is presented in **Figure 3(a)**. The emission blue shifts when we decrease the dot height and increase their Al content. A spectral shift from 340 nm to 260 nm is demonstrated while maintaining approximately the same spectral linewidth. The acceleration voltage (V_A) determines the penetration depth of the electrons in the structure, which depends mostly on the material density. The thickness of the SL was initially decided by assuming that the sample behaves similar to a planar structure with the same geometry along the growth axis. However, in a NW ensemble, the average material density is smaller, and there is a risk of electron channeling when the direction of impinging electrons is perpendicular to the silicon substrate. To assess the relevance of these phenomena, we have studied the variation of the CL spectra as a function of V_A, as shown in **Figure 3(b)**. If the emission spectra are normalized to their maximum, the emission from the GaN base becomes visible only for V_A > 5 kV. This implies that the NW ensemble is compact enough to prevent important deviations of their behavior with respect to planar structures.

Finally, we have assessed the IQE of the samples by analyzing the variation of their emission, either photoluminescence (PL) or CL, as a function of temperature. As an example, **Figure 4(a)** displays the evolution of the PL spectrum as a function of temperature for a sample containing an $Al_{0.1}Ga_{0.9}N$/AlN SL (0.75 nm GaN / 3.75 nm AlN). **Figure 4(b)** depicts the luminescence intensity as a function of the inverse temperature measured both by PL and CL, showing that there is no significant difference between the two measuring techniques.

The IQE is often estimated as the ratio of the luminescence intensity at room temperature and at low temperature: IQE ≈ *I*(300 K) / *I*(0 K). However, it should be kept in mind that this expression assumes that *I*(0 K) is not affected by non-radiative processes. Overestimation of the IQE can happen if non-radiative recombination paths are active at low temperature, but also if the pumping intensity is high enough to saturate non-radiative recombination paths at high temperature. The measured IQE is also higher under pulsed excitation, due to the difference in the behavior of radiative and non-radiative recombinations with respect to time. To get a reliable measurement, our PL experiments were performed under continuous wave excitation, using very low power densities (10 μW pumping power focused on a spot with a diameter around 100 μm). The fact that the luminescence intensity is almost constant up to 50 K is an indication that non-radiative recombination is negligible at low temperature (5 K). Therefore, we can assume that the expression IQE ≈ *I*(300 K) / *I*(5 K) is valid in our case. Following this reasoning, the sample emitting around 285 nm in **figure 4** presents IQE > 40%. This value increases up to IQE > 60% for samples emitting around 330 nm, and it decreases to ≈ 22% at 258 nm.

3. Conclusion

In summary, we have demonstrated the synthesis and characterization of $Al_xGa_{1-x}N$/AlN (x = 0, 0.1) quantum dot SLs on GaN NWs designed for application in electron-pumped UV sources.

The $Al_xGa_{1-x}N$/AlN active region is 400 nm long (88 periods of quantum dots), long enough to collect the electron-hole pairs generated by an electron beam with an acceleration voltage ≤ 5 kV. The NWs are grown using plasma-assisted MBE on n-type Si(111) wafers using a low temperature AlN nucleation layer. To adjust the spectral response, we have varied the dot/barrier thickness ratio and the Al content in the dots. By growing the $Al_xGa_{1-x}N$ quantum dots under N-rich conditions and the AlN barriers at the stoichiometry, we obtain SLs with a regular periodicity along the whole active region. In all the cases, the room temperature emission is dominated by a single spectral line that can be tuned from 340 nm (IQE > 60%), to 286 nm (IQE = 44 %) and 258 nm (IQE = 22%).

4. Experimental Section

X-ray diffraction (XRD) measurements where performed in a Rigaku SmartLab x-ray diffractometer using a 4 bounce Ge(220) monochromator and a long plate collimator of 0.228° for the secondary optics.

The morphology of the as-grown NW ensemble was studied by field-emission scanning electron microscopy (SEM) using a Zeiss Ultra 55 microscope.

Detailed structural studies were conducted using high-resolution transmission electron microscopy (HR-TEM) and high-angle annular dark-field scanning transmission electron microscopy (HAADF-STEM) performed on a probe-corrected FEI Titan Themis microscope operated at 200 kV.

Cathodoluminescence (CL) experiments were performed using a field-emission SEM FEI Inspect F50 equipped with a low-temperature Gatan stage to cool the sample down to 6 K, and with an IHR550 spectrometer.

Photoluminescence (PL) spectra were obtained by excitation with a frequency-doubled continuous-wave solid-state laser (λ = 244 nm), with an optical power of ≈ 10 μW focused on

a spot with a diameter of ≈ 100 µm. The sample was mounted on a cold-finger cryostat, and its emission was collected by a Jobin Yvon HR460 monochromator equipped with a UV-enhanced charge-coupled device (CCD) camera.

Acknowledgements

This work is supported by the French National Research Agency (ANR) via the UVLASE program (ANR-18-CE24-0014), and by the Auvergne-Rhône-Alpes region (grant PEAPLE). This project has also received funding from the European Research Council under the European Union's H2020 Research and Innovation programme via the e-See project (grant #758385). We also acknowledge technical support from F. Jourdan, Y. Curé and Y. Genuist. We benefited from the access to the technological platform NanoCarac of CEA-Minatech Grenoble in collaboration with the IRIG-LEMMA group.

Received: ((will be filled in by the editorial staff))
Revised: ((will be filled in by the editorial staff))
Published online: ((will be filled in by the editorial staff))

References

[1] M. A. Würtele, T. Kolbe, M. Lipsz, A. Külberg, M. Weyers, M. Kneissl, M. Jekel, *Water Research* **2011**, *45*, 1481.

[2] R. Collazo, S. Mita, J. Xie, A. Rice, J. Tweedie, R. Dalmau, Z. Sitar, *physica status solidi (c)* **2011**, *8*, 2031.

[3] M. L. Nakarmi, K. H. Kim, M. Khizar, Z. Y. Fan, J. Y. Lin, H. X. Jiang, *Appl. Phys. Lett.* **2005**, *86*, 092108.

[4] Y. Nagasawa, A. Hirano, *Applied Sciences* **2018**, *8*, 1264.

[5] T. Oto, R. G. Banal, K. Kataoka, M. Funato, Y. Kawakami, *Nature Photonics* **2010**, *4*, 767.

[6] T. Matsumoto, S. Iwayama, T. Saito, Y. Kawakami, F. Kubo, H. Amano, *Optics Express* **2012**, *20*, 24320.

[7] Y. Shimahara, H. Miyake, K. Hiramatsu, F. Fukuyo, T. Okada, H. Takaoka, H. Yoshida, *Applied Physics Express* **2011**, *4*, 042103.

[8] S. V. Ivanov, V. N. Jmerik, D. V. Nechaev, V. I. Kozlovsky, M. D. Tiberi, *physica status solidi (a)* **2015**, *212*, 1011.

[9] Y. Wang, X. Rong, S. Ivanov, V. Jmerik, Z. Chen, H. Wang, T. Wang, P. Wang, P. Jin, Y. Chen, V. Kozlovsky, D. Sviridov, M. Zverev, E. Zhdanova, N. Gamov, V. Studenov, H. Miyake, H. Li, S. Guo, X. Yang, F. Xu, T. Yu, Z. Qin, W. Ge, B. Shen, X. Wang, *Advanced Optical Materials* **2019**, *7*, 1801763.

[10] T. Hayashi, Y. Kawase, N. Nagata, T. Senga, S. Iwayama, M. Iwaya, T. Takeuchi, S. Kamiyama, I. Akasaki, T. Matsumoto, *Scientific Reports* **2017**, *7*, 2944.

[11] T. Wunderer, J. Jeschke, Z. Yang, M. Teepe, M. Batres, B. Vancil, N. Johnson, *IEEE Photonics Technology Letters* **2017**, *29*, 1344.

[12] M. Djavid, Z. Mi, *Appl. Phys. Lett.* **2016**, *108*, 051102.

[13] M. Beeler, C. B. Lim, P. Hille, J. Bleuse, J. Schörmann, M. de la Mata, J. Arbiol, M. Eickhoff, E. Monroy, *Phys. Rev. B* **2015**, *91*, 205440.

[14] L. F. Zagonel, S. Mazzucco, M. Tencé, K. March, R. Bernard, B. Laslier, G. Jacopin, M. Tchernycheva, L. Rigutti, F. H. Julien, R. Songmuang, M. Kociak, *Nano Letters* **2011**, *11*, 568.

[15] C. Himwas, M. den Hertog, L. S. Dang, E. Monroy, R. Songmuang, *Applied Physics Letters* **2014**, *105*, 241908.

[16] L. Rigutti, J. Teubert, G. Jacopin, F. Fortuna, M. Tchernycheva, A. De Luna Bugallo, F. H. Julien, F. Furtmayr, M. Stutzmann, M. Eickhoff, *Physical Review B* **2010**, *82*, 235308.

[17] F. Furtmayr, J. Teubert, P. Becker, S. Conesa-Boj, J. R. Morante, A. Chernikov, S. Schäfer, S. Chatterjee, J. Arbiol, M. Eickhoff, *Physical Review B* **2011**, *84*, 205303.

[18] S. D. Carnevale, J. Yang, P. J. Phillips, M. J. Mills, R. C. Myers, *Nano Lett.* **2011**, *11*, 866.

[19] C. Rivera, U. Jahn, T. Flissikowski, J. Pau, E. Muñoz, H. T. Grahn, *Physical Review B* **2007**, *75*, 045316.

[20] L. F. Zagonel, L. Rigutti, M. Tchernycheva, G. Jacopin, R. Songmuang, M. Kociak, *Nanotechnology* **2012**, *23*, 455205.

[21] A. Ajay, C. B. Lim, D. A. Browne, J. Polaczynski, E. Bellet-Amalric, M. I. den Hertog, E. Monroy, *physica status solidi (b)* **2017**, *254*, 1600734.

[22] M. Musolino, A. Tahraoui, S. Fernández-Garrido, O. Brandt, A. Trampert, L. Geelhaar, H. Riechert, *Nanotechnology* **2015**, *26*, 085605.

[23] K. K. Sabelfeld, V. M. Kaganer, F. Limbach, P. Dogan, O. Brandt, L. Geelhaar, H. Riechert, *Appl. Phys. Lett.* **2013**, *103*, 133105.

[24] R. Songmuang, T. Ben, B. Daudin, D. González, E. Monroy, *Nanotechnology* **2010**, *21*, 295605.

[25] R. Calarco, R. J. Meijers, R. K. Debnath, T. Stoica, E. Sutter, Hans. Lüth, *Nano Lett.* **2007**, *7*, 2248.

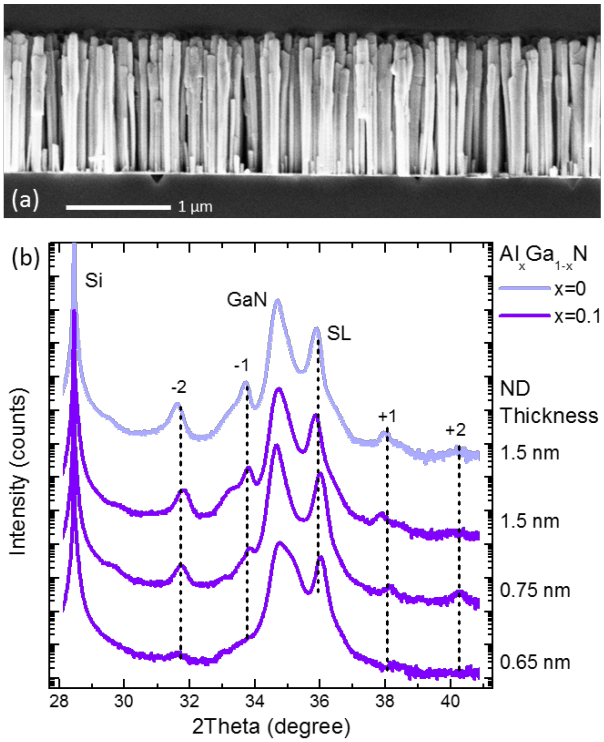

Figure 1. (a) Cross-section SEM view of a sample containing GaN NWs with a SL consisting of 88 periods of $Al_{0.1}Ga_{0.9}N$/AlN (0.75 nm/3.75 nm). (b) XRD θ–2θ scans of the (0002) reflection of GaN NWs containing an 88-period $Al_xGa_{1-x}N$/AlN SL. The Al concentration is color-coded and the thickness of the quantum dots is indicated on the right side of the figure. The diffractograms are vertically shifted for clarity.

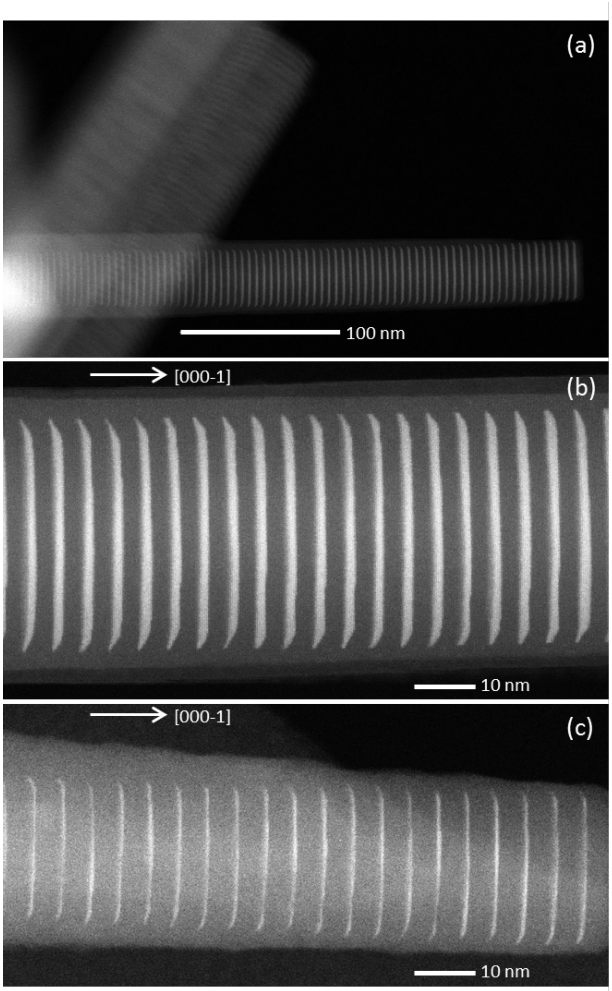

Figure 2. (a) HAADF-STEM image of dispersed NWs containing 88 periods of GaN/AlN (1.5 nm/3.0 nm). The bright contrast is GaN and the darker contrast represents AlN. (b) High-magnification HAADF-STEM image of a NW containing 88 periods of GaN/AlN (1.5 nm/3.0 nm). (c) High-magnification HAADF-STEM image of a NW containing 88 periods of $Al_{0.1}Ga_{0.9}N$/AlN (0.65 nm/3.85 nm).

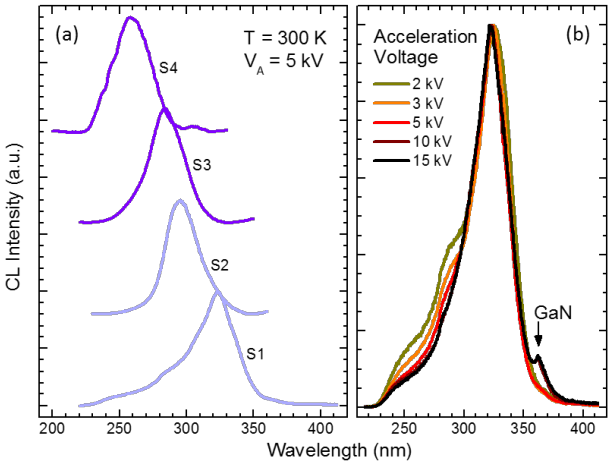

Figure 3. Room-temperature CL measurements of NWs containing an 88-period AlGaN/AlN SL. (a) Measurements performed at an acceleration voltage $V_A = 5$ kV of samples with the following SL structures: S1: 1.5 nm GaN / 3.0 nm AlN, S2: 0.75 nm GaN / 3.75 nm AlN, S3: 0.75 nm $Al_{0.1}Ga_{0.9}N$ / 3.75 nm AlN, S4: 0.65 nm $Al_{0.1}Ga_{0.9}N$ / 3.85 nm AlN. (b) Normalized CL spectra of the S3 structure as a function of the accelerating voltage. The emission from the GaN stem of the NWs is only resolved for $V_A > 5$ kV.

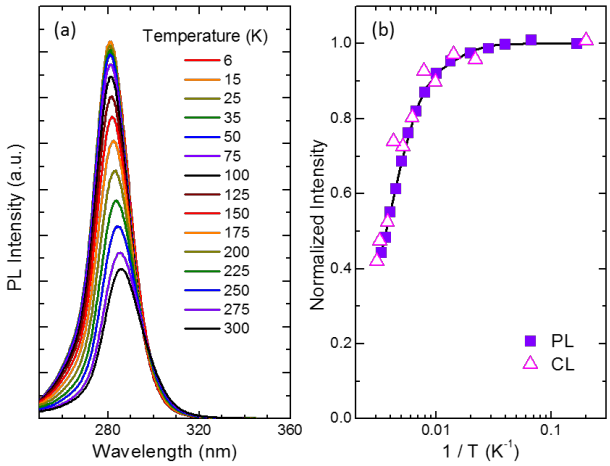

Figure 4. (a) Variation of the PL spectra as a function of temperature (sample SA2: 0.75 nm $Al_{0.1}Ga_{0.9}N$ / 3.75 nm AlN). (b) Variation of the PL and CL intensities of SA2 as a function of the inverse temperature, normalized to their value at low temperature. The solid line is a fit to $1/[1 + A \exp(-E_a/(kT))]$, where $E_a = 48 \pm 4$ meV is a thermal activation energy, kT is the thermal energy and $A = 7 \pm 2$ is a fitting constant.

ToC entry:

This paper describes the fabrication of AlGaN/AlN quantum dot superlattices on GaN nanowires for application in electron-pumped UV sources. The active region is designed to collect the carriers generated by an electron beam with an acceleration voltage of 5 kV. The emission is tuned in the 340 to 258 nm range by varying the dot/barrier thickness ratio and the Al content in the dots.

Keywords: ultraviolet, nanowires, AlGaN, quantum dot, lamp

I. Dimkou, A. Harikumar, A. Ajay, F. Donatini, E. Bellet-Amalric, M. I. den Hertog, S. T. Purcell, and E. Monroy*

Design of AlGaN/AlN dot-in-a-wire heterostructures for electron-pumped UV emitters

ToC figure: